Fabry–Perot filter using grating structures

Yu-Sheng Lin, Chong Pei Ho, Kah How Koh, and Chengkuo Lee*

Department of Electrical & Computer Engineering, National University of Singapore, 4 Engineering Drive 3, Singapore 117576
Corresponding author: elelc@nus.edu.sg

Grating structures are designed at the inner wall of the Fabry–Perot (FP) resonator to enhance the performance of an FP optical filter. The rectangular grating or triangular grating (TG) structures allows the light to be propagated effectively through the FP resonator. Attributed to the grating structures, the spectrum intensity of a FP resonator with grating structures is calculated to be 4.5-fold higher than that of a FP resonator with slot. In addition, the Q-factor of the resonant peak for a FP resonator with hybrid TG structure and two slots is 9.5-fold and 4.7-fold higher than that of a FP resonator with one slot and TG configurations, respectively.   © 2013 Optical Society of America
    OCIS codes: 120.2230, 120.2440, 230.1480, 230.5750.

Fabry–Perot (FP) optical filters are well-known for playing an important role in remote sensing, biomedical imaging, and displays applications [1]. FP filters have also been enabling optical devices with wavelength selective properties in optical telecommunication systems, which demand narrow full width at half-maximum (FWHM), wide free spectrum range (FSR) and wide dynamic range. To enhance the Q-factor and finesse (F) of a linear-configured FP filter, waveguide-based FP filters [2,3], photonics crystal tapered cavities [4–6], or ring resonators [7] are often considered. However, these methods often suffer propagation losses in integrated optical structures. These propagation losses originate from three main different sources, which are coupling to radiation modes, intrinsic absorption in the material, and scattering due to imperfections in the fabrication of the waveguide [8].

In order to achieve high-Q resonance in a FP cavity in the absence of large number of Bragg layers, a high refractive index (RI) contrast among the dielectric stack is often needed. By utilizing Si/air distributed Bragg reflector (DBR) mirrors with high index contrast, compact FP cavities can be realized that are suitable for wavelength division multiplexing, sensors, and nonlinear optics applications [1]. For FP filter that utilizes free space light propagation, the light propagating through the Si/air/Si DBR mirrors suffer serious reflection between Si/air interface, resulting in propagation losses. Therefore, it is important to devise new designs to allow the light to resonate effectively in the FP cavity and propagate through the resonators, hence enhancing the performance of the optical filter. Here, we propose to integrate the antireflection grating (ARG) structures on the inner walls of the FP resonator. ARG surfaces were first discovered in nature while inspecting the moth's eyes by Bernhard in 1963 [9]. The basic principle of ARG surface lies in the RI of the surface layer varying gradually from air to substrate, and thus effectively suppresses the specular reflectance at the interface of the two media [10,11]. Unlike typical gratings, ARG surfaces are constructed such that only the zero-orders of reflected and transmitted light can be propagated, while the higher diffraction orders are evanescent. Thus, the aberration of the optical wavefront can be avoided at the ARG surfaces and hence reduces the propagation loss [12,13].

In this Letter, novel FP filters are proposed, while comparison with typical FP filter, i.e., resonator with slot, is also investigated. We employ rectangular grating (RG) and triangular grating (TG) structures and integrate them with FP resonator in order to achieve high-Q Si/air DBR mirrors.

Figure 1(a) shows the typical design of a FP resonator, including Si/air/Si slabs with $P = 1.5$ periods being used in present investigation in order to compare designs with top views of the FP resonators in slot, RG, and TG configurations as shown in Figs. 1(b)–1(d), respectively. The width of Si slab ($W_{Si} = 770$ nm) and air ($W_{air} = 875$ nm) are calculated by using the equation $W_{eff} = m \cdot \lambda_0/4 \cdot n_{eff}$, where λ_0, n_{eff}, and m are wavelength in free space, effective RI and an integer, respectively. Using a transfer matrix approach [7], the DBR reflectance was calculated, assuming $\lambda_{center} = 3500$ nm and $n_{eff} = 3.428$. The FP filters utilized DBRs with $\lambda/4$ air gaps and $m \cdot \lambda_0/4 \cdot n_{eff}$ wide silicon sections ($m = 3$).

Figure 2(a) shows the spectra results of the FP resonator with slot, RG and TG configurations, respectively. The intensity of the FP resonator with RG was enhanced 1.9-fold higher when compared with that of the FP resonator with slot, while the intensity of the FP resonator with TG was enhanced 4.5-fold and 2.3-fold higher than those of FP resonator with slot and RG, respectively. The performance of a FP filter is characterized by its Q-factor and finesse, which are expressed as [14],
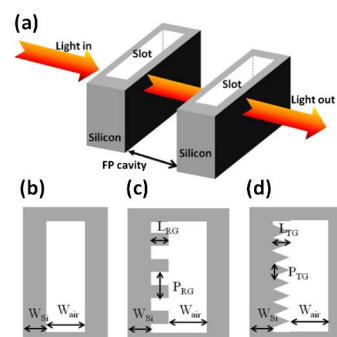

Fig. 1.   (Color online) (a) Schematic diagram of FP resonators; (b)–(d) are top views of FP resonator with slot, rectangular grating (RG), and triangular grating (TG) structures, respectively. (Where $W_{Si} = 770$ nm, $W_{air} = 875$ nm, $L_{RG} = L_{TG}$ is varied from 474 to 1422 nm, P_{RG} is varied from 500 to 4000 nm, and P_{TG} is from 250 to 1000 nm, respectively.)
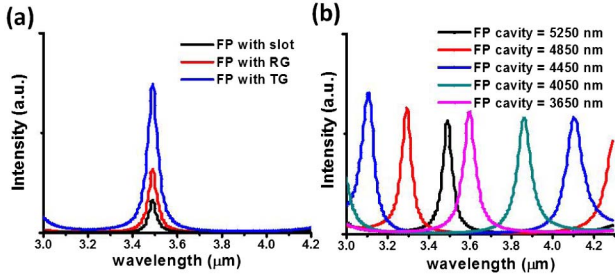
Fig. 2. (Color online) (a) Spectra of FP with slot, RG, and TG structures, respectively, at initial state (FP cavity is 5250 nm); and (b) spectra of FP filter with TG structures when shrunk FP cavity by 400 nm per step.

$$Q = \frac{\lambda}{\text{FWHM}} = \frac{\lambda_0 F}{\text{FSR}}, \qquad (1)$$

$$F(R) = \frac{\pi \sqrt{R(\lambda)}}{1 - R(\lambda)}, \qquad (2)$$

where $R(\lambda)$ is the wavelength dependent reflectivity. The FWHM of spectra of these three types of FP filters are 45 nm (slot), 35 nm (RG), and 30 nm (TG), respectively. Q-factors and F, calculated using Eqs. (1) and (2), for these three FP filters are 77 (slot), 100 (RG), and 116 (TG) for Q-factors, 25.7 (slot), 33.3 (RG), and 38.6 (TG) for F, respectively. The FSR is given by $\text{FSR} = \lambda_0^2/(2 \cdot n_c \cdot L_c)$ for $\lambda_0 \ll n_c \cdot L_c$ (where n_c and L_c are the RI and the cavity length, respectively). Assuming $\lambda_0 = 3500$ nm and $n_c = 1$, we obtained $\text{FSR} = 1166.6$ nm for cavity lengths $L_c = 5250$ nm. This calculation result is comparable with modeling results as shown in Fig. 2(b), which shows the FP spectra when cavity length is shrunk by 400 nm per step. This optical performance improvement can be attributed to the ARG structures superimposed on the FP resonator. The reflectance and transmittance of propagation light are expressed by Eq. (3), where n_0 is RI of air, n_s is RI of Si, and n_{eff} is effective RI of ARG. The n_{eff} can be derived from Eq. (4) [13], where f is the filling factor of the ARG structures, which is the volume percentage of the ARG structures in the FP resonator. The uniqueness of effective medium approximation is that it can be extended to multiple numbers of constituent layers expressed by Eq. (5) [13]. The role of ARG, therefore, is to increase the amount of light being transmitted to the DRB mirrors and resonating in the FP cavities.

$$R = \left| \frac{(n_0 n_s - n_{\text{eff}}^2)}{(n_0 n_s + n_{\text{eff}}^2)} \right|^2, \qquad T = \frac{4 n_0 n_s n_{\text{eff}}^2}{|(n_0 n_s + n_{\text{eff}}^2)|^2}, \qquad (3)$$

$$n_{\text{eff}} = \left| \frac{[1 - f + f n_s^2][f + (1 - f)n_s^2] + n_s^2}{2[f + (1 - f)n_s^2]} \right|^{1/2}, \qquad (4)$$

$$\sum_{i=1}^{N} f_i \frac{(n_i^2 - n_{\text{eff}}^2)}{(n_i^2 + 2n_{\text{eff}}^2)} = 0. \qquad (5)$$

Optimization of the FP filter designs for RG and TG structures is also made with respect to grating periods (P_{RG} and P_{TG}) and lengths (L_{RG} and L_{TG}), with reference to the gradient refractive index (GRIN) theory [12,13]. Figures 3(a) and 3(b) show the spectra of the FP resonator with RG and TG, respectively, with both configurations having the same grating length ($L_{\text{RG}} = L_{\text{TG}} = 474$ nm). When the grating period increases, the decadence degree of optical intensity of the FP resonator with TG is smaller than that with RG as shown in Fig. 3(c). The reason is due to the RI gradient of the FP resonator with RG being lower than that of the FP resonator with TG, causing the scattering loss to be higher in the former compared to the latter [13]. Moreover, the optical intensity of the FP resonator with RG decays faster than that of the FP resonator with TG when grating pitch size is larger than 750 nm. Figure 3(d) shows the optical intensity of FP with RG and TG versus different grating length and period. The variation of optical intensity is 2.29% for TG periods of 250, 500, and 750 nm. This value is lower than that for the periods of RG (which variation of optical intensity is 3.98% in the period 500–4000 nm). For TG lengths of 474, 948, and 1422 nm, the variation of optical intensity is 8.39%. This indicates that the tolerance of fabrication is large for the range of grating periods from 250 to 750 nm and grating lengths from 474 to 1422 nm. That means optical losses due to fabrication imperfections should be minimal, while significant losses are due to beam divergence within the air gaps of the DBR [15].

The Q-factor of FP filter can be enhanced by using more periods of Si/air DBR mirrors [16]. However, the optical intensity will be reduced, although the Q-factor is improved. Here, we proposed an additional hybrid design to enhance the Q-factor, while improving the optical intensity as well. The results in Fig. 3 have shown that the optical performance of FP filter with TG structures is better than that of FP filter with RG structures. In this consideration, we further optimized the performance of the FP filter by hybrid integration of the TG structures with one and two Si/air periods in FP resonator, as shown
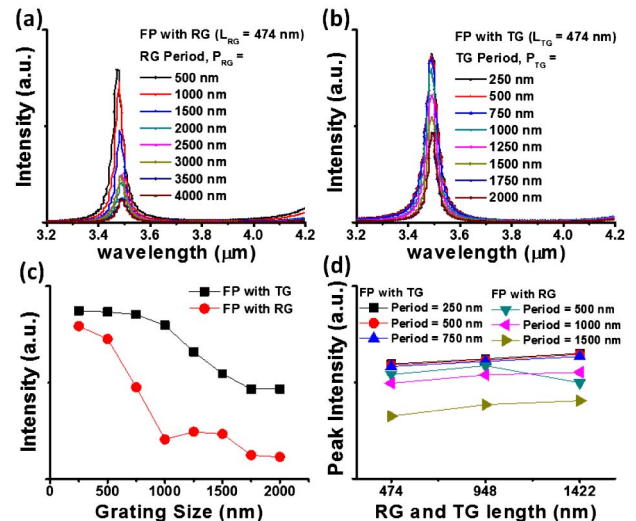

Fig. 3. (Color online) Spectra of FP filters with (a) RG; (b) TG of different periods, peak intensity of FP filters with RG and TG for different; (c) grating size; and (d) grating length.
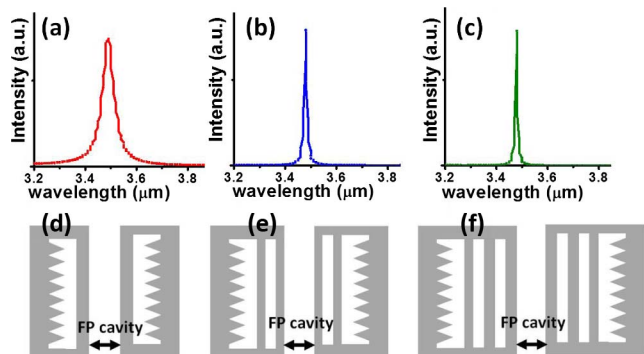
Fig. 4. (Color online) (a)–(c) Spectra of FP resonator with TG, TG plus one slot, and TG plus two slots, respectively. (FP cavity is 5250 nm); (d)–(f) are schematic top view drawings of FP resonators in configurations (a)–(c), respectively.

Table 1. Result Summary for the FP Filters of Five Different Configurations

Configurations	FWHM	Q	F	Normalized Peak Intensity (a.u.)
1 slot	60.0	58.3	20	0.223
RG	45.0	77.7	26	0.423
TG	30.0	116.6	39	1
TG+ 1 slot	10.5	333.3	111	0.142
TG+ 2 slots	6.3	555.5	185	0.018

in Fig. 4. Figure 4(a) shows the spectrum of the FP resonator with TG structures, whose Q-factor is 116.6 and F is 39. Such configuration yield performance that is 2-fold higher than that of the FP resonator with one slot. When TG structures are integrated into FP resonators with one [Fig. 4(e)] and two [Fig. 4(f)] Si/air periods, the Q-factor and F are enhanced 2.8-fold [Fig. 4(b)] and 4.7-fold [Fig. 4(c)], respectively, when compared with that of a FP resonator with TG structures only [Fig. 4(a)]. The improved Q-factor and F are attributed to the increased light intensity, resulting in narrower FWHM, as shown by the results in Figs. 2 and 3. Table 1 summarizes the results obtained from all the five configurations investigated in this Letter.

By integrating the FP resonator with antireflective grating structures, novel FP filters with high optical intensity, high Q-factor, and high finesse become plausible. Such integration of ARG structures into FP filters can enhance their optical performance due to GRIN on the sidewalls of the FP resonator. The optical intensity of FP resonator with TG was improved 4.5-fold higher when compared with that of slot structure. In the case for Q-factor, the hybrid FP resonator with TG and two slots was enhanced 9.5-fold and 4.7-fold better than those values of FP resonator with one slot and FP resonator with TG, respectively. The finesse of the hybrid FP resonator with TG and two slots ($F = 39$) is 1.95-fold higher than that of FP with slot ($F = 20$). These novel FP optical filters can be further integrated with microelectromechanical system actuators, offering tuning possibility in the full spectra range.

References
1. N. Gat, Proc. SPIE **4056**, 50 (2000).
2. C. A. Barrios, V. R. Almeida, R. R. Panepucci, B. S. Schmidt, and M. Lipson, IEEE Photon. Technol. Lett. **16**, 506 (2004).
3. M. W. Pruessner, T. H. Stievater, and W. S. Rabinovich, Appl. Phys. Lett. **92**, 081101 (2008).
4. P. Lalanne and J. P. Hugonin, IEEE J. Quantum Electron. **39**, 1430 (2003).
5. A. R. M. Zain, N. P. Johnson, M. Sorel, and R. M. D. L. Rue, Opt. Express **16**, 12084 (2008).
6. A. R. M. Zain, N. P. Johnson, M. Sorel, and R. M. D. L. Rue, IEEE Photon. Technol. Lett. **22**, 610 (2010).
7. B. E. Little, S. T. Chu, H. A. Haus, J. Foresi, and J.-P. Laine, J. Lightwave Technol. **15**, 998 (1997).
8. M. Lipson, IEEE J. Lightwave Technol. **23**, 4222 (2005).
9. C. G. Bernhard, G. Höglund, and D. Ottoson, J. Insect Physiol. **9**, 573 (1963).
10. B.-J. Bae, S.-H. Hong, E.-J. Hong, H. Lee, and G.-Y. Jung, Jpn. J. Appl. Phys. **48**, 010207 (2009).
11. Y. S. Lin, W. C. Hsu, K. C. Huang, and J. A. Yeh, Appl. Surf. Sci. **258**, 2 (2011).
12. D. H. Raguin and G. M. Morris, Appl. Opt. **32**, 1154 (1993).
13. W. H. Southwell, J. Opt. Soc. Am. A **8**, 549 (1991).
14. J. Masson, R. St-Gelais, A. Poulin, and Y. A. Peter, IEEE J. Quantum Electron. **46**, 1313 (2010).
15. C. F. R. Mateus, C. H. Chang, L. Chrostowski, S. Yang, D. Sun, R. Pathak, and C. J. Chang-Hasnain, IEEE Photon. Technol. Lett. **14**, 819 (2002).
16. A. Lipson and E. M. Yeatman, Opt. Lett. **31**, 395 (2006).